Dynamics of the Gas-Phase Reactions of Fluoride Ions with Chloromethane

Laurence A. Angel and Kent M. Ervin*

Department of Chemistry and Chemical Physics Program, University of Nevada, Reno, Nevada 89557

Received: November 27, 2000; In Final Form: February 12, 2001

Guided ion beam tandem mass spectrometry techniques are used to examine the competing chemical dynamics of reactions of fluoride ions with chloromethane in the center-of-mass collision energy range 0.05−30 eV. The exothermic bimolecular nucleophilic substitution (S_N2) reaction $F^- + CH_3Cl \rightarrow CH_3F + Cl^-$ predominates at the lowest collision energies (0.05−0.1 eV) but decreases by a factor of ∼100 over the range 0.1−2 eV. Two endothermic product channels are detected at collision energies ∼1−20 eV, corresponding to proton transfer to form $HF + CH_2Cl^-$ and chlorine abstraction to form $CH_3 + FCl^-$. The threshold energy for the proton-transfer reaction is $E_0 = 97 \pm 9$ kJ/mol, which yields $\Delta_{acid}H_{298}(CH_3Cl) \leq 1653 \pm 9$ kJ/mol and $EA_0(CH_2Cl) \geq 0.77 \pm 0.14$ eV. The threshold energy for the chlorine abstraction reaction to form FCl^- is $E_0 = 170 \pm 40$ kJ/mol, which yields $EA_0(FCl) \geq 2.6 \pm 0.4$ eV. Potential energy surfaces for the three reaction paths are calculated using the coupled cluster and density functional theory methods at the CCSD(T)/aug-cc-pVDZ and B3LYP/aug-cc-pVDZ levels. Geometry optimizations of stationary points along the surfaces show that a hydrogen-bonded $F^-\cdots H-CH_2Cl$ complex is 5 kJ/mol lower in energy than the C_{3v} $F^-\cdots CH_3Cl$ complex. An additional feature observed in the Cl^- reaction cross section at collision energies above 2 eV is attributed to further dissociation of CH_2Cl^- and FCl^- products.

Introduction

There have been extensive studies, both experimental and theoretical,[1−3] on gas-phase S_N2 nucleophilic substitution in halomethanes, reaction 1. The minimum potential energy surface

$$X^- + CH_3Y \rightarrow XCH_3 + Y^- \qquad (1)$$

for this reaction is a double-well potential,[4−6] with the two potential energy minima corresponding to formation of the entrance and exit ion−dipole complexes $X^-\cdots CH_3Y$ and $XCH_3\cdots Y^-$. The two ion−dipole complexes are separated by a central potential energy barrier which corresponds to the five-coordinate $[X-CH_3-Y]^-$ transition state. However, when the S_N2 reaction is highly exothermic as in the case of reaction 2,

$$F^- + CH_3Cl \rightarrow FCH_3 + Cl^- \qquad (2)$$

the entrance ion−dipole, $F^-\cdots CH_3Cl$ (**1a** in Figure 1), has a very shallow potential energy minimum and a small central barrier to the transition state $[F-CH_3-Cl]^-$ (**1b**). The small well on the potential energy surface may yield a short-lived prereactive intermediate in which energy redistribution is on a longer time scale than the S_N2 reaction, resulting in nonstatistical reaction kinetics. Previous investigations[7−9] have postulated that the entrance ion−dipole complex is important at low energies but has less influence on the reaction at collision energies above 0.2 eV. In experimental studies,[7] the S_N2 reaction rate constants were measured versus relative translational energy and CH_3Cl temperature in a variable temperature selected ion flow drift tube (VT-SIFDT) experiment. The thermal rate constants have been modeled by collision theory including an orientational effect for the reaction,[7] by statistical theory,[8] and by a classical trajectory study.[9] From these analyses, the reaction rate behavior has been attributed to the influence of ion−dipole capture at collision energies 0.01−0.1 eV, with the reactants forming the ion−dipole complex, $F^-\cdots CH_3Cl$ (**1a**). The $F^-\cdots CH_3Cl$ ion−dipole complex (**1a**) initiates the S_N2 reaction, which then passes

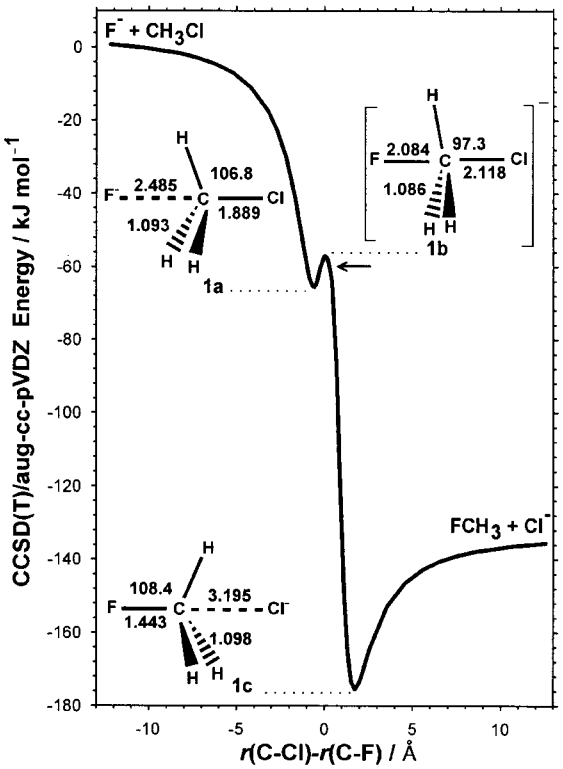

Figure 1. Potential energy surface for reaction 2 in C_{3v} symmetry. The energy relative to reactants calculated at the CCSD(T)/aug-cc-pVDZ level is plotted versus the difference between the C−Cl and C−F bond lengths. The arrow marks the point of the central point of inversion, where the methyl group is planar.

* Corresponding author. E-mail: ervin@chem.unr.edu.

10.1021/jp0042866 CCC: $20.00
Published on Web 04/03/2001

along the PES shown in Figure 1 through the $[F-CH_3-Cl]^-$ transition state (**1b**) and the exit ion−dipole $FCH_3\cdots Cl^-$ intermediate (**1c**). As collision energies increase above 0.2 eV, however, the ion−dipole attraction is overcome by the greater translational energy of the reactants, resulting in a direct reaction mechanism. The direct collisions require collision orientations with alignment for the S_N2 backside attack, resulting in a rapid decrease in the S_N2 reaction rate in the collision energy region 0.2−1 eV.

Flowing afterglow selected ion flow tube experiments have given thermal rate constants of $(1.3-1.4) \times 10^{-9}$ cm^3 s^{-1} for reaction 2 at 300 K,[10,11] which compare to the calculated collision rate coefficient[12] by the ratio $k_{exp}/k_{col} = 0.56-0.61$. The partitioning of the S_N2 reaction exothermicity into relative translational energy and internal energy of the products has also been investigated using kinetic energy release Fourier transform ion cyclotron resonance spectroscopy[13] and by direct ab initio dynamics calculations.[14] Both studies reported high translational excitation of the S_N2 products, with the theoretical work[14] also reporting vibrational excitation of the C−F stretching mode of the CH_3F product. Microsolvation of reaction 2 with a single water molecule has also been investigated by direct ab initio dynamics calculations in order to elucidate a detailed reaction mechanism.[15]

Reports of gas-phase reactions of halide ions with halomethanes other than S_N2 are more limited. Dihalide ions XY^- were observed in separate guided ion beam experiments—the $ClBr^-$ ion from the reaction $Cl^- + CH_3Br$ in the center-of-mass collision energy range 2−15 eV[16] and the Cl_2^- ion from the reaction $Cl^- + CH_3Cl$, exhibiting a threshold energy above the calculated potential barrier height.[17] Ion beam experiments by Vietzke and co-workers[18] measured the collision energy dependence of the products H^-, FBr^-, and CH_2Br^- from the reaction $Br^- + CH_3F$, and FI^- and CH_2I^- from $I^- + CH_3F$. There have been no experimental reports to our knowledge of a competing proton transfer for reaction 1, where X and Y are both halogens, although an ab initio investigation[19] of the reaction $F^- + CH_3F$ reported finding a hydrogen-bonded $F^-\cdot\cdot\cdot H-CH_2F$ intermediate near the energy of the ion−dipole $F^-\cdots CH_3F$ intermediate.

Here we show that in the collision energy range 1−30 eV the endothermic reactions 3 and 4 can be driven by translational energy in competition with reaction 2. The competing reactions

$$F^- + CH_3Cl \rightarrow HF + CH_2Cl^- \quad (3)$$

$$F^- + CH_3Cl \rightarrow CH_3 + FCl^- \quad (4)$$

2−4 are assessed by examining the reaction cross section behavior in the center-of-mass (c.m.) collision energy region 0.05−30 eV. Reactions 3 and 4 have measurable threshold energies that are compared with previously published thermochemical values. To help investigate the microscopic reaction mechanisms, coupled cluster and density functional theory (DFT) techniques are used to calculate the potential energy surfaces (PES) for reactions 2−4.

Experimental Methods and Results

A detailed description of the guided ion beam tandem mass spectrometer has been published previously,[17] and only an outline will be presented here. Helium buffer gas with a trace of the precursor gas hexafluorobenzene, C_6F_6, flows at a rate of 5.0 L/s (STP) into a flow tube reactor (flowing afterglow) at a pressure of 50 Pa. A microwave discharge source produces fluoride anions from the hexafluorobenzene. The anions are sampled at the end of the flow tube through a 1.5 mm aperture nose cone, and then shaped, focused, and accelerated by a series of lenses. A magnetic mass spectrometer mass selects the F^- ions, and they are guided by a further series of lenses and a 90° quadrupole bender lens to an octopole radio frequency ion trap. The F^- ions are decelerated to a desired translational energy and injected into the octopole. Situated at the center of the octopole is a reaction cell where the reactant gas chloromethane is introduced via a leak valve. The energy of collision between the fluoride ions and the neutral chloromethane is controlled by the dc potential difference between the flow tube ion source and the octopole. The octopole also provides a radial effective potential well for highly efficient collection of the scattered anionic reactants and products. The anions are extracted from the octopole and injected into a quadrupole mass spectrometer where they are mass analyzed. Ion intensities are detected by a collision dynode/particle multiplier operated in negative-ion pulse counting mode. The pulses are counted by a multichannel scalar board controlled by a computer.

Absolute reaction cross sections are determined as a function of collision energy by scanning the ion energy (octopole dc potential) and counting the reactant and product ions for predetermined dwell times. The laboratory ion energy is measured using retarding potential analysis, confirmed by time-of-flight measurements, and converted to relative collision energy, E, in the c.m. frame. Ion counts due to background signals occurring outside the reaction cell are also collected and subtracted from the total. All cross sections are measured at three pressures in the range $(5-20) \times 10^{-5}$ mbar. The results are extrapolated to zero pressure by a least-squares linear regression, ensuring that all the reported cross sections are in the single-collision limit.

The threshold behavior of the cross section, $\sigma(E)$, is modeled using an empirical threshold law,[17,20−22]

$$\sigma(E) = \sigma_0 \sum_i g_i [E + E_i - E_0]^N / E \quad (5)$$

where E_i is the internal energy of reactant state i with fractional thermal population g_i corresponding to a Maxwell−Boltzmann distribution at 300 K, σ_0 and N are adjustable parameters, and E_0 is the 0 K reaction threshold energy. Experimental[23] vibrational frequencies and rotational constants of CH_3Cl are used for the sum over reactant internal energies. The rovibrational density of states is calculated by the Beyer−Swinehart Stein−Rabinovitch direct count algorithm.[24−26] Finally, eq 5 is convoluted over the experimental collision energy distributions,[27,28] as described previously.[20] These calculations are performed using the CRUNCH data analysis program.[29]

The reported error limits are propagated from individual sources of uncertainty (assuming they are independent of each other) and represent ±2 combined standard uncertainties[30] or an approximate 95% confidence level. Uncertainties are included for the determination of the ion beam energy zero, the reproducibility of data taken on separate occasions, the vibrational frequencies, the least-squares fit of eq 5, and the consistency of the fit using different energy ranges.

The experimental reaction cross sections from 0.05 to 30 eV c.m. are shown in Figure 2. Three products ions are observed; Cl^- at low energies and CH_2Cl^- and FCl^- at higher energies. The cross section behavior is primarily the result of reactions 2−4. The S_N2 reaction cross section is greatest ($\sim 100 \times 10^{-16}$ cm^2) at the lowest collision energies (0.05 eV) and decreases by a factor of ~100 over the range 0.5−2 eV. The proton-

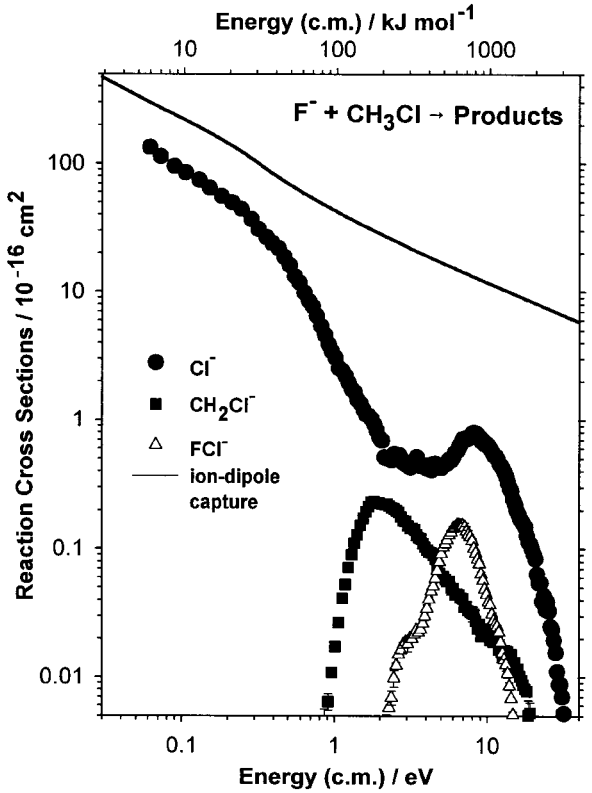

Figure 2. Cross sections for the product ions Cl^-, CH_2Cl^-, and FCl^- from the reaction of $F^- + CH_3Cl$ as a function of collision energy in the center-of-mass frame. The calculated ion−dipole capture cross section[38] is shown as the solid line.

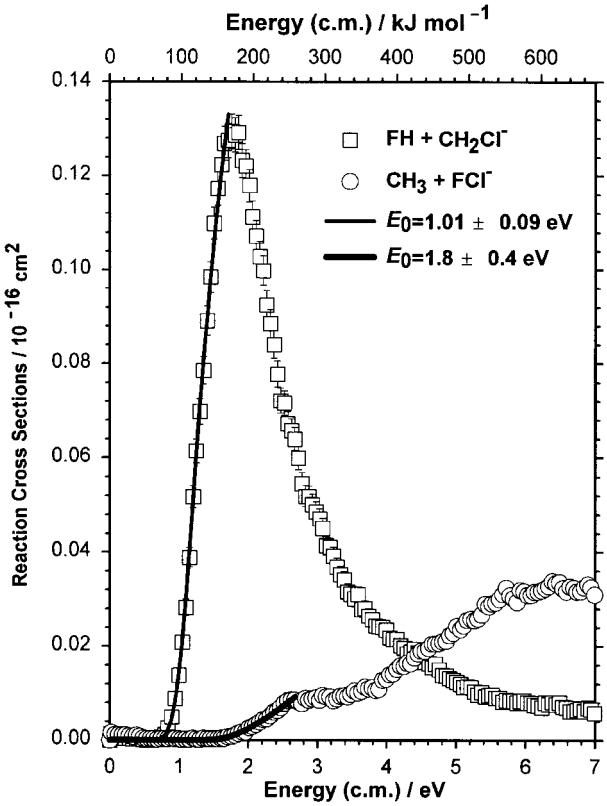

Figure 3. Cross sections for the threshold regions for reactions 3 and 4 as a function of collision energy in the center-of-mass frame. The squares and circles are experimental data and the solid lines are the fits of eq 5 convoluted as described in the text.

transfer reaction cross section rises from an apparent center-of-mass collision threshold energy of 0.9 eV, rising to a maximum at 2 eV and declines to the experimental detection limit through the region 2−20 eV. The FCl^- reaction cross section exhibits two features, an initial rise of the cross section to 0.02×10^{-16} cm^2 starting at an apparent energy of 2 eV, followed by a further increase in the cross section to 0.2×10^{-16} cm^2, originating at approximately 3.5 eV.

At collision energies above 2 eV c.m. the Cl^- cross section exhibits a secondary feature. The Cl^- cross section exhibits a plateau region from 2 to 6 eV followed by an increase and a peak at 8 eV c.m. The onsets of these features correlate with the peaks in the cross sections of the CH_2Cl^- and FCl^- channels. The Cl^- cross section behavior at these collision energies is probably the result of reactions 6 and 7 becoming energetically possible. The inverse relationship between the Cl^- cross section

$$F^- + CH_3Cl \rightarrow Cl^- + [CH_2 + HF] \quad (6)$$

$$F^- + CH_3Cl \rightarrow Cl^- + [F + CH_3] \quad (7)$$

and the cross sections of CH_2Cl^- and FCl^- are thus explained, because reactions 6 and 7 represent the further dissociation of the CH_2Cl^- and FCl^- ions made initially by reactions 3 and 4, respectively.

Fits of the empirical threshold law to the rising experimental cross section data for reactions 3 and 4 are shown in Figure 3. Threshold energies for the endothermic reactions 3 and 4 are obtained using eq 5 as $E_0(3) = 97 \pm 9$ kJ/mol (1.01 ± 0.09 eV) and $E_0(4) = 170 \pm 40$ kJ/mol (1.8 ± 0.4 eV) and are compared with other experiments and theory in Table 1. The proton-transfer reaction exhibits a steep initial cross section rise, allowing a good empirical threshold fit. The small initial rise in the FCl^- experimental cross section, however, results in a relatively large uncertainty in the threshold fit for reaction 4. From the reaction threshold energies $\Delta_{acid}H_{298}(CH_3Cl) \leq 1653 \pm 9$ kJ/mol, $EA_0(CH_2Cl) \geq 0.77 \pm 0.14$ eV and $EA_0(FCl) \geq 2.6 \pm 0.4$ eV are obtained (Table 2). The conversion from 0 to 298 K for the gas-phase acidity is calculated using the rigid-

TABLE 1: Threshold Energies and Enthalpies of Reactions at 0 K (kJ mol^{-1})

reaction products	E_0 (this work)	Δ_rH_0 (exp)[a]	G3[b]	B3LYP/ aug-cc-pVDZ[c]
$F^- + CH_3Cl$	0	0	0	0
$Cl^- + CH_3F$		-129 ± 8[d]	−134	−136
$CH_2Cl^- + HF$	$\leq 97 \pm 9$	94 ± 18[e]	103	111
$FCl^- + CH_3$	$\leq 170 \pm 40$	190 ± 20[f]	192	147
		274 ± 29[g]		
$Cl^- + CH_2 + HF$		212 ± 4	208	
$Cl^- + F + CH_3$		323 ± 1	318	
$CH_2F^- + HCl$		180 ± 19[h]	186	
$CHCl^- + HF + H$		459 ± 30[i]	470	
$CHCl^- + H_2 + F$		593 ± 30[i]	603	
$FCl^- + CH + H_2$		634 ± 20[f]	632	
$FCl^- + CH_2 + H$		646 ± 21[f]	649	

[a] Enthalpies of reaction calculated using enthalpies of formation from Gurvich et al.,[47] except as noted. [b] Calculated here or taken from http://chemistry.anl.gov/compmat/g3theory.htm.[60] [c] Energies corrected for zero-point energy. [d] Calculated using $\Delta_fH_0(CH_3F) = -225 \pm 8$ kJ/mol estimated by Kolesov,[61] which agrees with theoretical calculations by Berry et al.[62] [e] Calculated using $EA(CH_2Cl) = 0.80 \pm 0.16$ eV determined by Bartmess[40] from work by Ingemann and Nibbering.[41] [f] Calculated using $EA(FCl) = 2.37 \pm 0.21$ eV from Dudin et al.[54] [g] Calculated using $EA(FCl) = 1.5 \pm 0.3$ eV from Dispert and Lacmann[55] or Harland and Thynne.[53] [h] Calculated using $\Delta_fH_0(CH_2F^-) = -53 \pm 19$ kJ/mol determined by Bartmess[40] from work by Graul et al.[63] [i] Calculated using $EA(CHCl) = 1.210 \pm 0.005$ eV from Gilles et al.[64]

TABLE 2: Electron Affinities and Dissociation Energies (eV)

species XCl	EA_0 (this work)	EA (exp)	EA_0 (G3 theory)	$D_0(X\text{-}Cl^-)$ (this work)
CH_2Cl	$\geq 0.77 \pm 0.14$	0.80 ± 0.16[a]	0.70	$\geq 1.2 \pm 0.1$
FCl	$\geq 2.6 \pm 0.4$	2.37 ± 0.21[b]	2.34	$\geq 1.6 \pm 0.4$
		1.5 ± 0.3[c]		

[a] Bartmess[40] from work by Ingemann and Nibbering.[41] [b] Dudin et al.[54] [c] Dispert and Lacmann[55] and Harland and Thynne.[53]

TABLE 3: Stationary Point Energies ΔH_0 (kJ mol^{-1})[a]

complex or transition state		B3LYP/aug-cc-pVDZ[b]	CCSD(T)[c]	CCSD(T)/aug-cc-pVDZ[b]
1a $F^-\cdots CH_3Cl$	ion-dipole, C_{3v}	−68.1	−66.1(−66.1)	−69.0
1b $[F\cdots CH_3\cdots Cl]^-$	transition state, C_{3v}	−67.6	−53.8(−53.3)	−61.0
1c $FH_3C\cdots Cl^-$	ion-dipole, C_{3v}	−170.6	−173.1(−177.9)	−174.2
4a $F^-\cdots H-CH_2Cl$	H-bonded, C_s	−73.0		−74.2
5a $F^-\cdots Cl-CH_3$	halo-bonded, C_{3v}	−9.0		
5b $F^-\cdots ClCH_3$	transition state, C_{3v}	9.7		
6a $[ClF\cdots CH_3]^-$	transition state, C_1	98.6		
6b $Cl^-\cdots H-CH_2F$	H-bonded, C_1	−161.0		

[a] Energies relative to $F^- + CH_3Cl$ reactants. [b] This work. Values include B3LYP/aug-cc-pVDZ zero-point energies. [c] Botschwina et al.[37] Values include B3LYP/aug-cc-pVDZ zero-point energies with the original reported values in parentheses.

rotor harmonic-oscillator approximation using standard statistical mechanics formulas.[23]

Theoretical Methods and Potential Energy Surfaces

Density functional theory (DFT), Gaussian-3 (G3), and coupled cluster calculations were performed using Gaussian 98[31] to help interpret the experimental results. Potential energy surfaces (PES) and zero-point energy (ZPE) corrected stationary points were calculated for reactions 3 and 4 at the B3LYP/aug-cc-pVDZ level. The performance of density functional theory in describing reaction 1 has been examined previously.[32,33] The reports concluded that reasonable values are obtained by DFT for the complexation energies, but the central barrier heights for the reactions are significantly underestimated when compared with G2(+) or experimental results. Consequently, the coupled cluster method CCSD(T)/aug-cc-pVDZ was used to calculate the potential energy surface for reaction 2. However, CCSD(T) frequency calculations were not feasible with our computer resources. Stationary points are confirmed at the B3LYP/aug-cc-pVDZ level with frequencies at the same level. B3LYP/aug-cc-pVDZ reaction enthalpies for the reactions 2−4 are shown in Table 1 and stationary state energies are listed in Table 3. The 0 Kelvin reaction enthalpies for possible products resulting from $F^- + CH_3Cl$, and the electron affinities of CH_2Cl and FCl were also calculated at the G3 level, and are shown in Tables 1 and 2. Both the G3 reaction enthalpies and electron affinities show good agreement with the experimental values. Comparison of the B3LYP/aug-cc-pVDZ reaction enthalpies with the G3 and experimental values show reasonable correlation for reactions 2 and 3, but a considerably lower Δ_4H_0 value for reaction 4. The stability of two-center three-electron bond systems, which includes FCl^-, has been reported to be overestimated by density functional methods.[33] The overestimating of the relative stability of FCl^- will result in an underestimation of Δ_4H_0, as observed in Table 1.

The PES shown in Figure 1 was calculated for the S_N2 reaction 2 in C_{3v} symmetry using CCSD(T)/aug-cc-pVDZ. The geometries of the three stationary points, (**1a**) the entrance ion−dipole complex, (**1b**) the transition state, and (**1c**) the exit ion−dipole complex, are shown in Figure 1. The PES exhibits a small central barrier height (ΔH_{cent}) of 8 kJ/mol, with correction for ZPE, relative to the entrance channel complex. Previous studies using HF, MP2, QCISD, CCSD(T), and G2(+) have shown a wide variation of results for the central barrier of reaction 2, with values of 0−26 kJ/mol.[8,9,34−37] The authors[37] of the calculations at the highest level of theory, CCSD(T) with a large basis set, recommend 13.8 ± 1.3 kJ/mol after considering basis set superposition error and additional electron correlation and basis set effects but without correction for ZPE. Also shown in Figure 1 is the central point of inversion, where the C−H bonds are at 90° to the $[F-C-Cl]^-$ axis. The inversion point is beyond the central barrier along the C_{3v} reaction coordinate and approximately 4 kJ/mol lower in energy.

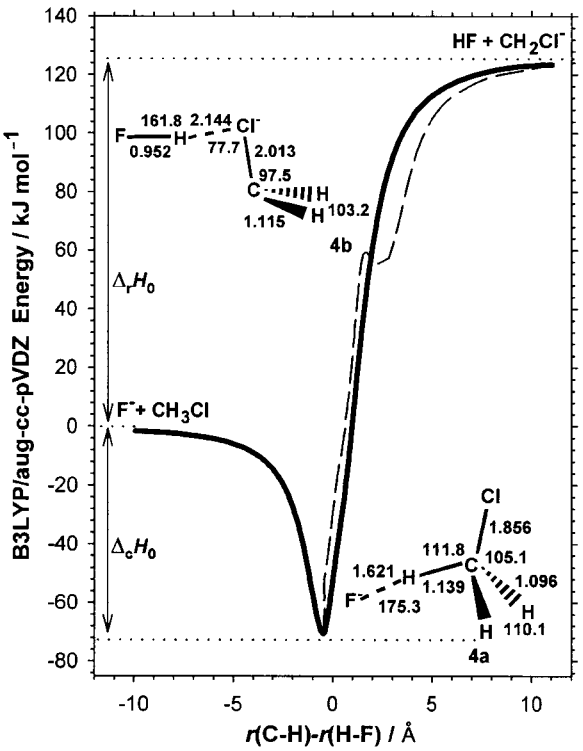

Figure 4. Potential energy surface for reaction 3 in C_s symmetry. The energy relative to reactants calculated at the B3LYP/aug-cc-pVDZ level is plotted versus the difference between the C−H and H−F bond lengths. The dashed line is an alternative PES in C_s symmetry, which is a result of hydrogen bonding between the products (see text).

Potential energy surfaces for reactions 3 and 4 were examined using the more economical B3LYP/aug-cc-pVDZ level. The PES for proton transfer (reaction 3) in C_s symmetry is shown in Figure 4. The reaction surface (solid line) shows a single well potential with an initial attractive surface into a minimum well and then a steep exit channel out to products. The bottom of the well corresponds to the formation of the strong hydrogen-bound $F^-\cdots H-CH_2Cl$ C_s complex (**4a**). When fully optimized and corrected for ZPE, the hydrogen-bound intermediate has a complexation energy of $\Delta_cH_0 = -73.0$ kJ/mol, making it 4.9 kJ/mol more stable than the S_N2 C_{3v} ion−dipole complex (**1a**). The hydrogen-bound complex is also calculated to be the more stable prereactive intermediate by 5.2 kJ/mol using the CCSD(T)/aug-cc-pVDZ method with ZPE corrections from DFT (Table 3). This is surprising, as previous trajectory, statistical, and dynamics studies[7−9,14,15] of reaction 2 have all used potential energy surfaces that have the C_{3v} ion−dipole complex as the lowest energy prereactive intermediate, without considering hydrogen-bonded geometries. The present work shows that a restricted C_{3v} ion−dipole analytical potential energy surface may

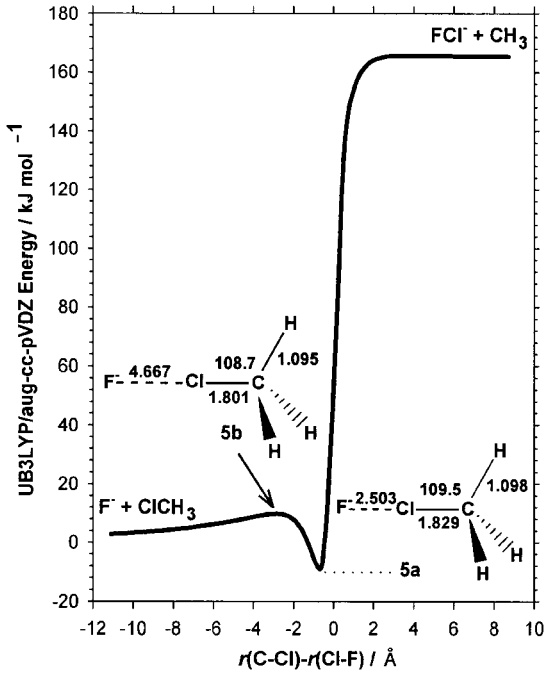

Figure 5. Potential energy surface for reaction 4 in C_{3v} symmetry. The energy relative to reactants calculated at the B3LYP/aug-cc-pVDZ level is plotted versus the difference between the C−Cl and Cl−F bond lengths.

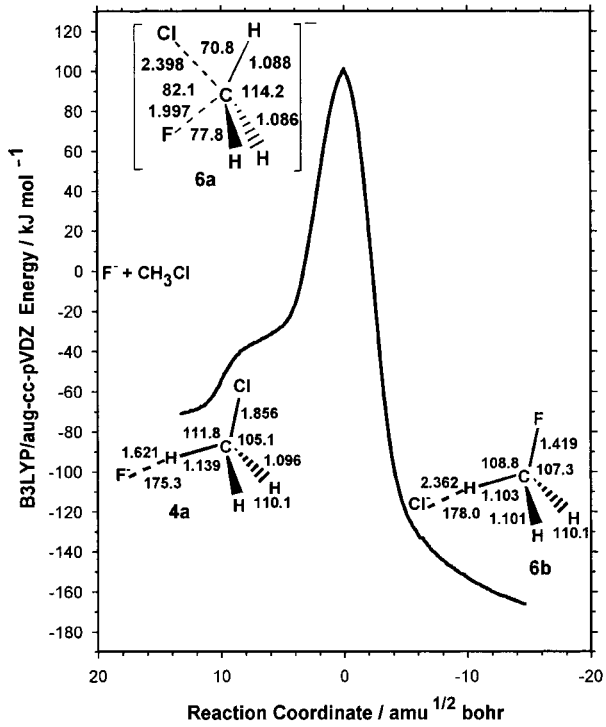

Figure 6. Potential energy along the intrinsic reaction coordinate for the front-side nucleophilic attack mechanism in C_1 symmetry. The energy relative to reactants calculated at the B3LYP/aug-cc-pVDZ level is plotted versus the intrinsic reaction coordinate (mass-weighted Cartesian coordinates).

be insufficient for describing a multidimensional PES for reaction 1, where either X = F or Y = F, because of the strong hydrogen-bonding propensity of fluoride. Calculations at the CCSD(T)/aug-cc-pVDZ level show that there is a barrier of less than 3 kJ/mol for rearrangement between **1a** and **4a**, smaller than the S_N2 barrier from **1a** to **1c**.

Figure 4 shows no barriers along the surface in excess of the 0 K reaction endothermicity, Δ_3H_0. However, the smooth exit path was achieved by restraining the Cl−C−H angle to 109° as the HF departs from the CH_2Cl^- ion at r(C−H) − r(H−F) distances greater than 5 Å. If the Cl−C−H angle is not constrained, the geometry optimizes to the PES shown by the dashed line in Figure 4. This alternative PES is a result of a hydrogen bonding interaction between CH_2Cl^- and HF. This surface is calculated by following geometry optimizations that lead from the products HF and the CH_2Cl^- down to several structurally similar local potential energy minima at approximately 55 kJ/mol (relative to F^- + CH_3Cl). A transition state structure (first-order saddle-point), with geometry shown in **4b**, is located 4 kJ/mol above these local minima and an intrinsic reaction coordinate (IRC) calculation connects this saddle point with the lowest local minimum and also with the minimum-energy $F^-\cdots H-CH_2Cl$ C_s complex (**4a**). Although we were unsuccessful in an attempt to find a unique minimum energy path between these two separate reaction paths, we cannot exclude the possibility that one exists.

The PES using B3LYP/aug-cc-pVDZ for the halophilic attack mechanism (reaction 4) with C_{3v} symmetry, $F^-\cdots Cl-CH_3$, is shown in Figure 5. The PES exhibits an initially repulsive entrance surface, passing over a saddle point to a shallow single well, corresponding to the minimum potential energy structure **5a**. Then a steep exit channel surface leads to FCl^- and CH_3 products. The entrance channel transition state, **5b**, lies 9.7 kJ/mol higher in ZPE-corrected energy than the reactants, at a $F^-\cdots ClCH_3$ distance of 4.7 Å. There is also a small, and possibly artifactual, excess barrier to the reaction enthalpy of only 0.5 kJ/mol as the products exit at $FCl^-\cdots CH_3$ distances of 5−10 Å in C_{3v} symmetry. To model the exit channel out to the correct products, the PES was calculated using the unrestricted method UB3LYP/aug-cc-pVDZ. This is necessary because the restricted B3LYP/aug-cc-pVDZ method dissociates into FCl^{2-} and CH_3^+ at much higher energies. The unrestricted wave function exhibits a considerable amount of spin contamination, however, so the results may have only qualitative significance. The lack of a significant barrier in excess of the endothermicity in Figure 5 suggests that the halophilic reaction could be responsible for the first rising feature of the FCl^- cross section originating from the thermodynamical threshold.

An intrinsic reaction coordinate (IRC) calculation at the B3LYP/aug-cc-pVDZ level for the front-side carbon attack mechanism with C_1 symmetry is shown in Figure 6. The C_1 symmetry transition state **6a** is 99 kJ/mol higher in zero-point corrected energy than the reactants F^- + CH_3Cl (Table 3). The IRC surface connects the transition state, **6a**, to two minimum hydrogen-bonded intermediates, **4a** and **6b**. An IRC calculation with C_s symmetry (not shown) connects to an equivalent minimum structure to **6b**, but no minimum was located on the side of structure **4a**. Instead, the C_s IRC dissociates back out to reactants F^- + CH_3Cl through a doubly hydrogen-bonded interaction. The C_1 IRC initially follows the same doubly hydrogen-bonded path as the C_s IRC but allows for a geometry rearrangement from the doubly to a singly hydrogen-bonded structure. This hydrogen-bonding rearrangement can be observed in Figure 6 as the sigmoidal curve in the lower part of the IRC connecting **6a** to **4a**. The $F^-\cdots H-CH_2Cl$ structure, **4a,** is the same structure located on the proton-transfer PES, which, as already discussed, is lower in energy than the S_N2 $F^-\cdots CH_3Cl$ ion−dipole complex, **1a**. The comparative complexation energies are shown in Table 3. In contrast, the IRC path leading to the $Cl^-\cdots H-CH_2F$ hydrogen-bonded complex, **6b**, is formed by only a single hydrogen-bond interaction, resulting in the smooth slope connecting **6a** and **6b**. Table 3 shows that **6b** has

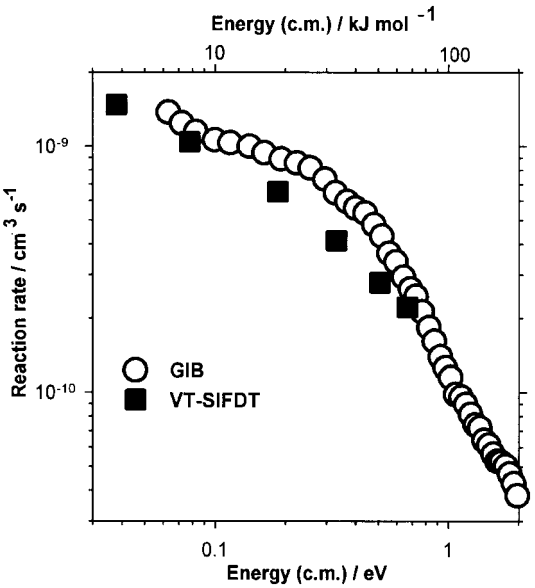

Figure 7. Comparison of the S_N2 guided ion beam cross section data with the VT-SIFDT results of Viggiano and co-workers.[7] The squares represent the drift tube rate coefficients as a function of the mean energy in the center-of-mass frame. The circles are the GIB cross sections from the present work converted to rate coefficients as described in the text.

a 9.6 kJ/mol weaker complexation energy than the related C_{3v} $FCH_3\cdots Cl$ ion−dipole complex, **1c**.

Discussion

S_N2 Reaction Cross Section Behavior. The only reaction product observed at apparent collision energies less than 0.9 eV c.m. is the Cl^- ion, produced by the S_N2 reaction. The reaction cross section exhibits a maximum of approximately 100×10^{-16} cm^2 at the lowest collision energies, below 0.1 eV. As collision energies increase from 0.5 to 2 eV, the S_N2 reaction cross section exhibits a steeper negative slope proportional to $E^{-2.0}$.

For comparison of our reaction cross section data with the measurements of $k(E)$ in VT-SIFDT experiments by Viggiano and co-workers,[7] we converted[20] our S_N2 cross sections to energy-dependent rate coefficients according to $k(\langle E\rangle) = \sigma(E_{cm})\text{-}v_{rel}$, where $v_{rel} = (2E_{cm}/\mu)^{1/2}$ is the relative collision velocity, $\langle E\rangle = E_{cm} + (3/2)\gamma k_B T$ is the mean energy of the distribution, $\mu = (M_{ion}M_{gas}/(M_{ion} + M_{gas})$ is the reduced mass, and $\gamma = M_{ion}/(M_{ion} + M_{gas})$. The comparison between the two sets of results, for the energy range 0.05−2 eV, is shown in Figure 7 and exhibits good agreement. The small deviations may be attributed to the different energy distributions of the two experiments. Modeling shows that the displaced Boltzmann distribution of drift tube experiments gives a less steep decline at the higher energies, which is consistent with the apparent crossing of the two sets of data approaching 1 eV.

Plotted with the experimental cross sections in Figure 2 is the calculated ion−dipole capture cross section.[38] The S_N2 experimental cross section approaches about 50% of the calculated collision cross section at the lowest energies,[38] consistent with thermal rate coefficients.[10,11] Comparison between the slopes of the Cl^- reaction cross section and the ion−dipole capture shows that the Cl^- cross section follows the slope of the ion−dipole capture much better in the low-energy region, 0.05−0.5 eV, than at collision energies 0.5−2 eV. The S_N2 behavior at these energies has previously been explained by Su et al.[7,9] to be partly influenced by the ion−dipole capture and the formation of the entrance $F^-\cdots CH_3Cl$ ion−dipole complex (Figure **1a**). The behavior is consistent with a reaction model postulated by Su et al.,[7−9] that at low collision energies the reaction cross section is controlled partly by the formation of the entrance ion−dipole $F^-\cdots CH_3Cl$, which has time to favorably align in the conventional S_N2 backside attack configuration (Fig. 1a). At higher energies, the reaction becomes more direct, and the reaction efficiency decreases rapidly. For a direct reaction, the initial encounter must have the correct orientation for the backside S_N2 mechanism to occur.

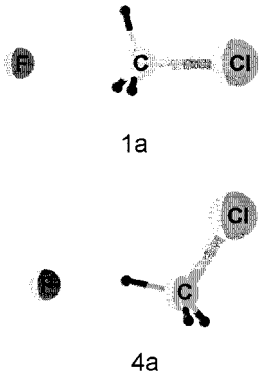

Figure 8. Comparison of the (**1a**) C_{3v} ion−dipole and (**4a**) C_s hydrogen-bonded minimum energy complexes.

The apparent propensity of F^- to form a hydrogen-bonded complex with CH_3Cl, as indicated by our calculations, was not recognized by earlier studies of reaction 2,[7−9,14,15,36,37] although $F^-\cdots HR$ hydrogen bonding is well-known.[39] For thermal and low collision energies, the additional influence of the three equivalent hydrogen-bonded complexes will increase the lifetime of the prereactive intermediate deepening the entrance well on a multidimensional PES. The structurally and energetically similar ion−dipole and hydrogen-bonded intermediates, compared in Figure 8, can easily interconvert at the available energies. CCSD(T) calculations indicate that only a small barrier (<3 kJ/mol) exists between the two species.

Proton-Transfer Reaction. Figure 2 shows that at collision energies above 0.9 eV a translationally driven proton-transfer reaction occurs resulting in the CH_2Cl^- ion. The empirical threshold fit to the rising reaction cross section is shown in Figure 3. The empirically measured 0 K threshold energy, E_0, for the proton-transfer reaction is 97 ± 9 kJ/mol (1.01 ± 0.09 eV). This value agrees well with the literature reaction thermochemistry, $\Delta_3H_0 = 94 \pm 18$ kJ/mol, Table 1. The uncertainty in the literature value of $EA_0(CH_2Cl) = 0.80 \pm 0.16$ eV[40,41] is the main contributor to the relatively large error bars in Δ_3H_0. G3 calculations, shown in Tables 1 and 2, yield values of $\Delta_3H_0 = 103$ kJ/mol and $EA_0(CH_2Cl) = 0.70$ eV, agreeing within the uncertainties with the experimental results. E_0 threshold energies are equal to the reaction enthalpy, ΔH_0, in the absence of any potential barriers along the reaction path or any dynamical barriers hindering the proton-transfer reaction.[42] An effective energy barrier for reaction 3 would result in E_0 being an upper limit for the Δ_3H_0 value. In Figure 4 both potential energy surfaces (solid and dashed lines) calculated for the proton-transfer reaction show that there are no intrinsic potential energy barriers in excess of the reaction enthalpy.

The alternative PES (dashed line) is not a unique minimum energy path but provides evidence that a proton-transfer reaction mechanism may exist where a torque of the CH_2Cl^- molecule to hydrogen bonding with the HF could result in a small dynamical exit restriction along the potential energy surface. The hydrogen bonding interaction could result in some trans-

lational energy from the departing HF and CH_2Cl^- products being converted into the rotation of the CH_2Cl^- ion. This small redistribution of energy may be enough to restrict product formation at or very near the threshold energy of the reaction. In previous guided ion beam bimolecular endoergic proton-transfer reactions, DeTuri et al.[42,43] found that the threshold energies derived from bimolecular proton-transfer reactions provide good agreement with the literature values when rotational energy is excluded from promoting the reaction. Accordingly, rotational energy has been excluded from the empirical threshold model (eq 5) used to calculate the threshold energy for reaction 3. However, instances of large dynamic barriers for proton transfer were also found, mainly for reactions where the complex is only weakly hydrogen-bonded.[43] The proton-transfer systems investigated by DeTuri et al., however, did not contain any electronegative atoms remote from the proton-transfer site and, therefore, the PES exit feature for reaction 3 investigated here was not present.

A "competitive shift" may also impede the proton-transfer reaction if the reaction mechanism shares an intermediate along its reaction path with the competing S_N2 reaction. However, as already discussed in the previous section, the S_N2 reaction is considered to proceed at energies above 0.5 eV through a direct collision model, without formation of a prereactive complex. The nominal intermediates for the two reactions correspond to the different structures compared in Figure 8. Unlike complex formation at the lowest collision energies, a direct mechanism at collision energies above 0.5 eV c.m. may not allow for exchange or competition.

Because of a possible dynamical constraint on energy transfer due to hydrogen bonding of the products and because of a possible competitive shift resulting from the exothermic S_N2 channel, the experimental proton-transfer threshold energy for reaction 3 is recommended as an upper limit to the 0 K reaction enthalpy, $\Delta_3H_0 \leq E_0(3) = 97 \pm 9$ kJ/mol. Using the E_0 value we can estimate $\Delta_{acid}H_{298}(CH_3Cl) \leq 1653 \pm 9$ kJ/mol from the relationship $E_0(3) \geq \Delta_3H_0 = \Delta_{acid}H_0(CH_3Cl) - \Delta_{acid}H_0(HF)$, where $\Delta_{acid}H_0(HF) = 1549.85 \pm 0.01$ kJ/mol.[44,45] The $\Delta_{acid}H_{298}(CH_3Cl) \leq 1653 \pm 9$ kJ/mol value is within the mutual error bars with $\Delta_{acid}H_{298}(CH_3Cl) = 1657 \pm 13$ kJ/mol from Ingemann and Nibbering[41] and $\Delta_{acid}H_{298}(CH_3Cl) = 1672 \pm 10$ kJ/mol determined by Henchman et al.[46] Also, $EA_0(CH_2Cl) \geq 0.77 \pm 0.14$ eV is derived from $EA_0(CH_2Cl) \geq -\Delta_fH_0(F^-) - \Delta_fH_0(CH_3Cl) + \Delta_fH_0(HF) + \Delta_fH_0(CH_2Cl) - E_0(3)$, using Δ_fH_0 values from Gurvich.[47] The comparison of $EA_0(CH_2Cl)$ with previous experimental and G3 theory values is shown in Table 2.

Chlorine Abstraction and Formation of FCl^-. At apparent collision energies above 2 eV, the formation of the dihalide ion FCl^- via Cl abstraction from CH_3Cl (reaction 4) is exhibited in Figures 2 and 3. The halide abstraction reaction implies that reactive collisions attack in either a front-side nucleophilic (at the carbon but adjacent to Cl) or front-side halophilic (chlorine end) mechanism. The double threshold for FCl^- feature is evidence that the reaction is proceeding through two reaction mechanisms. The initial reaction occurring at 2 eV is a less efficient mechanism at producing FCl^- than is the second mechanism above 3.5 eV. Table 1 shows ΔH_0 values for two additional reactions producing the FCl^- ion, corresponding to dissociation of the CH_3 molecule into $CH_2 + H$ and $CH + H_2$. Both reactions exhibit $\Delta H_0 > 6$ eV, however, which excludes them from either the first or second features in the FCl^- reaction cross section.

The dual reaction mechanism could be of the form of (1) halophilic attack at the chlorine of CH_3Cl, producing the C_{3v} complex **5a** and (2) nucleophilic attack at the front side of the carbon atom producing a C_1 complex **6a**, with both mechanisms leading to the products $FCl^- + CH_3$. The PES and IRC, shown in Figures 5 and 6, were calculated to investigate these two reaction mechanisms. However, only the halophilic attack reaction, Figure 5, provides a viable reaction pathway to the $FCl^- + CH_3$ products. Nucleophilic attack at the front side of the carbon, Figure 6, has a 99 kJ/mol energy barrier relative to the reactants $F^- + CH_3Cl$, and connects to two hydrogen-bonded complexes shown in **4a** and **6b** (rather than to a $FCl^- + CH_3$ asymptote).

The two hydrogen-bonded minima **4a** and **6b** located on the IRC and proton-transfer PES suggests that both front-side carbon attack and proton transfer may proceed from $F^-\cdots H-CH_2Cl$ hydrogen-bonded intermediates. If $F^-\cdots H-CH_2Cl$ hydrogen-bonded complexes are intermediates in proton transfer (3) then, likewise, $Cl^-\cdots H-CH_2F$ hydrogen-bonded complexes could be intermediates in a reaction that produces $CH_2F^- + HCl$. No measurable signal for the CH_2F^- ion was observed, however, even though Δ_rH_0 for the $F^- + CH_3Cl \rightarrow CH_2F^- + HCl$ reaction is only 180 ± 19 kJ/mol or approximately 1.9 eV (Table 1). The absence of the CH_2F^- ion is understandable on energetic grounds, however, with the $Cl^-\cdots H-CH_2F$ intermediate dissociating preferentially to the exothermic S_N2 products Cl^- and CH_3F, only 25 kJ/mol higher in energy than the complex, rather than climbing up a steep exit channel to $F^- + CH_3Cl \rightarrow CH_2F^- + HCl$ with an overall endothermicity of $\Delta_rH_0 = 180 \pm 19$ kJ/mol.

Bierbaum et al. interpreted experimental data on the S_N2 gas-phase reaction between the chloride ion and chloromethane as proceeding by a front-side chlorine attack mechanism,[48] although the data was later reevaluated as being consistent with a backside attack mechanism.[17] Subsequent ab initio work[49,50] identified a C_s saddle point for the same identity S_N2 reaction, corresponding to a front-side nucleophilic attack at the carbon atom. Further ab initio work by Glukhovtsev et al.[36] discussed the possible reaction intermediates in nonidentity S_N2 reactions, including F^- with chloromethane in both front-side and backside attack mechanisms. The inclusion of a new S_N2 front-side nucleophilic carbon attack mechanism, at collision energies above 99 kJ/mol (1 eV) might show up as a unique feature on the Cl^- cross section data in Figure 2. The Cl^- cross section data do in fact show new features at collision energies >2 eV c.m. At first there is a plateau region between 2 and 6 eV, which is followed by an increase and peak at a collision energy 8 eV before a tailing off at higher energies. These features, however, are at least as likely due to reactions 6 and 7 becoming energetically possible and contributing to the Cl^- cross section. At collision energies above 2 eV, the dissociation of the CH_2Cl^- into CH_2 and Cl^- (reaction 6), and the dissociation of FCl^- into F and Cl^- (reaction 7), both of which are discussed in more detail in the next section, become energetically possible and their probable inclusion in the Cl^- cross section makes it impossible to verify whether there is also a contribution from a S_N2 front-side attack mechanism at these energies.

An alternative explanation may be that direct energetic collisions above 3.6 eV, between the F^- ion and the Cl atom of CH_3Cl, result in impulsive rupture of the CH_3-Cl bond, $D_0(CH_3-Cl) = 3.558 \pm 0.008$ eV using values cited in Gurvich et al.[47] A rupture model partitions the energy from a direct collision between F^- ion and the Cl atom into the vibrational mode of the CH_3-Cl bond. The probable dissociation products are consistent with both the second feature on the FCl^- cross section and the similar feature, exhibited in Figure 2, by the

peak in the Cl^- cross section at 8 eV, already described above to be the result of reaction 7. Rupture of the CH_3-Cl bond by collision-induced dissociation (CID) could result in three possible product combinations: $F^- + Cl + CH_3$ from direct CID, $FCl^- + CH_3$ from CID accompanied by FCl^- bond formation, or $Cl^- + F + CH_3$ from CID accompanied by secondary dissociation of FCl^- and electron transfer. It is not possible to detect the F^- ion as a product from direct CID as it is indistinguishable in mass from the reactant ions. The other two species, however, are both detected with reaction cross section behavior providing evidence that they are related in this way. The FCl^- reaction cross section increases from approximately 3.6 eV to a peak at 6 eV, and as the cross section declines the Cl^- reaction cross section increases, rising to a peak at about 8 eV. This behavior is consistent with the FCl^- ion primarily being formed at c.m. collision energies > 3.6 eV, followed by dissociation into $F + Cl^-$ at energies > 6 eV. The Cl^- ion is formed preferentially because EA(Cl) = 3.6 eV is larger than EA(F) = 3.4 eV.[51]

The threshold energy, E_0, for reaction 4 is measured at 170 ± 40 kJ/mol (1.8 ± 0.4 eV) from the fit of the empirical threshold law shown in Figure 3. The large error bars are mainly a result of the large uncertainty derived from the empirical threshold fit (eq 5) to the small initial onset of the FCl^- reaction cross section. However, the value is precise enough to distinguish between previously published electron affinity (EA) values for FCl.[51−54] We calculate $EA_0(FCl) \geq 249 \pm 40$ kJ/mol (2.6 ± 0.4 eV), shown in Table 2, using $EA_0(FCl) \geq -\Delta_f H_0(F^-) - \Delta_f H_0(CH_3Cl) + \Delta_f H_0(CH_3) + \Delta_f H_0(FCl) - E_0(4)$ with $\Delta_f H_0$ values from Gurvich et al.[47] and our experimentally measured threshold value. Even as a lower limit, our EA measurement excludes the literature values EA(FCl) = 1.5 ± 0.3 eV from Dispert and Lacmann[55] and Harland and Thynne.[53] However, the $EA_0(FCl) = 2.37 \pm 0.21$ eV determined by Dudin et al.[54] agrees within the error bars of our measured $EA_0(FCl) \geq 2.6 \pm 0.4$ eV.

Both the experimental procedures,[52,53] which determined EA(FCl) = 1.5 ± 0.3 eV incorporated possibly large errors in their experimental appearance energy (AE) determination. The electron impact of SF_5Cl measurement by Harland and Thynne was evaluated from the process $SF_5Cl + e^- \rightarrow FCl^- + SF_2 + 2F$, with an appearance energy $AE(FCl^-) = 7.6 \pm 0.1$ eV, $\Delta_f H_{298}(SF_5Cl) = -10.9$ eV, $\Delta_f H_{298}(FCl) = -0.6$ eV, and $\Delta_f H_{298}(SF_2) = -2.8$ eV. The $\Delta_f H_{298}$ values are in reasonable agreement with more recently evaluated $\Delta_f H_{298}$ values from Gurvich et al.,[47] although later work[54] reevaluated the EA value with $\Delta_f H_0(SF_2) = -1.42$ eV, resulting in $EA_0(FCl) = 2.86$ eV. Early electron impact appearance energy measurements are well-known in their unreliability because of the difficulty in characterizing the electron energy and product energy distributions.[56] Moreover, high-energy products, such as FCl^- in the above experiment, are subject to major kinetic shifts and competitive shifts from lower energy product channels. This latter problem is certainly a possible cause of error in the above work as there are lower energy SF_5^-, SF_4^-, F^-, and Cl^- channels in competition with the high energy FCl^- product.

The report by Dispert and Lacmann estimated EA(FCl) = 1.5 ± 0.3 eV by measuring the threshold energy for the appearance of FCl^- and Cl_2^- from an electron-transfer reaction between neutral K and CCl_3F, using $EA(FCl) = AE(FCl^-) - AE(Cl_2^-) + EA(CCl_2)$. Both appearance energies were measured (coincidently) at 8.2 ± 0.3 eV. Using a recent value for $EA(CCl_2) = 1.603 \pm 0.008$ eV,[57] one obtains EA(FCl) = 1.6 ± 0.4 eV. The low calculated EA(FCl) is probably due to FCl^- and CCl_2^- again being high-energy channels subject to kinetic and competitive shifts from low-energy $CFCl_3^-$, Cl^-, Cl_2^-, $CFCl_2^-$, and F^- channels. Both experiments[52,53] described above also used parent species, SF_5Cl and CCl_3F, which contain no F−Cl bond, resulting in an extra complication to the reaction mechanism used to derive the EA.

The $EA_0(FCl) = 2.37 \pm 0.21$ eV, measured by Dudin et al.,[54] is in better agreement with our work, although it is also an electron impact appearance energy measurement. The value $AE(FCl^-) = 0.38 \pm 0.05$ eV was measured from the process $ClF_3 + e^- \rightarrow FCl^- + 2F$ and the EA calculated using $\Delta_f H_0$ values in good agreement with more recent values from Gurvich.[47] The higher electron affinity is also supported by ab initio calculations by Nguyen and Ha[58] and Van Huis et al.,[59] although the latter work calculated a relatively wide range of values from different DFT methods, ranging from 1.94 to 2.94 eV, and mistakenly concluded in supporting the reevaluated Harland and Thynne[53,54] value of 2.86 eV rather than the reported experimental value of 2.37 ± 0.21 eV.[54] Further support for the high $EA_0(FCl)$ value comes from our calculations using the G3 method.[31] At the G3 level, $EA_0(FCl) = 2.34$ eV, in good agreement with Dudin et al.[54] and our own result. The G3 EA value was also used to calculate the enthalpy change for the Cl abstraction reaction, using additional G3 heat of formation values previously calculated by Pople and co-workers.[60] The 0 K enthalpy change of reaction 4 was determined as $\Delta_4 H_0 =$ 192 kJ/mol (1.98 eV), shown in Table 1 and agrees within the uncertainty of our experimental $E_0(4) = 170 \pm 40$ kJ/mol. Table 1 also shows the G3 values for a wide range of enthalpies of reaction products resulting from $F^- + CH_3Cl$. There is overall good agreement between the experimentally determined ΔH_0 values and the calculated G3 values for all the reactions, providing additional confidence in the G3 value of $EA_0(FCl) = 2.34$ eV. In any case, our threshold results definitively exclude the accepted[51] value of $EA_0(FCl) \approx 1.5$ eV as being too low.

Cl^- Products above 2 eV. Two additional reactions, (6) and (7), become energetically possible above 2.2 and 3.3 eV, respectively.[47] The Cl^- reaction cross section behavior in Figure 2 exhibits possible contributions from both these reactions. The new Cl^- cross section behavior coincides with the same c.m. energy at which the cross section of CH_2Cl^- starts to decrease, giving additional support that reaction 6 is the initial contributor. Using our experimentally determined $\Delta_3 H_0 \leq 97 \pm 9$ kJ/mol and the $\Delta_6 H_0 = 212 \pm 4$ kJ/mol,[47] we calculate $D_0(CH_2-Cl^-) \geq 115 \pm 10$ kJ/mol (1.2 ± 0.1 eV), shown in Table 2.

The plateau feature in the Cl^- cross section continues to about 6 eV and is followed by an increase and a broad peak region in the Cl^- cross section, at energies 6−20 eV. This additional Cl^- cross section feature suggests that reaction 7 is also contributing to the formation of Cl^- ions at collision energies above 3.3 eV. The reaction enthalpy, $\Delta_7 H_0$, is equal to the sum of $\Delta_4 H_0$ and the dissociation energy of the halide ion FCl^-. Using our experimentally determined $\Delta_4 H_0 \leq 170 \pm 40$ kJ/mol and $\Delta_7 H_0 = 323 \pm 1$ kJ/mol,[47] we calculate $D_0(F-Cl^-) \geq 153 \pm 40$ kJ/mol (1.6 ± 0.4 eV), in agreement with values of 1.62 and 1.66 eV calculated at the $B3LYP/DZP^{2+}$ and $BP86/DZP^{2+}$ levels, respectively, by Van Huis et al.[59] Initially, the contribution of reaction 7 is limited because its precursor reaction 4 has a very small initial reaction cross section. At energies above 6 eV, as already described, the influence is much greater and the subsequent Cl^- cross section rise is related to the second feature of the FCl^- cross section where impulsively breaking the CH_3-Cl bond may become important in the reaction mechanism.

Conclusions

Three independent reactions (reactions 2−4) have been detected by guided ion beam techniques in the c.m. collision energy range 0.05−30 eV. The exothermic S_N2 reaction is most efficient at the lowest collision energies (0.05−0.1 eV) with the reaction cross section decreasing by approximately a factor of 100 over the energy range 0.1−2 eV. This behavior has been observed before[7,9] and has been explained by the backside attack orientation criterion needed for efficient S_N2 reaction. As collision energies increase, ion−dipole complex formation and alignment along the backside attack coordinate decrease with a corresponding decrease in the S_N2 reaction cross section. At center-of-mass collision energies of 1−20 eV, both proton transfer and chlorine abstraction reactions are observed, with measured threshold energies. The proton-transfer threshold energy is $E_0(3) = 1.01 \pm 0.09$ eV and recommended as an upper limit to the 0 K reaction enthalpy, $\Delta_3H_0 \leq 97 \pm 9$ kJ/mol, which gives $\Delta_{acid}H_{298}(CH_3Cl) \leq 1653 \pm 9$ kJ/mol and $EA_0(CH_2Cl) \geq 0.77 \pm 0.14$ eV. The experimental threshold energy for chlorine abstraction, $E_0(4) = 170 \pm 40$ eV (1.8 ± 0.4 eV), yields $EA_0(FCl) \geq 2.6 \pm 0.4$ eV. At collision energies above 2 eV, the Cl^- cross section is observed to increase again due to the probable dissociation of the CH_2Cl^- ion into Cl^- and CH_2 (reaction 6) and the FCl^- into Cl^- and F (reaction 7).

The experimental and theoretical data support the view that the gas-phase S_N2 reaction occurs primarily through the conventional backside attack route with inversion of configuration in the collision energy range 0.05−2 eV. The hydrogen-bound complex, **4a**, may help to stabilize prereactive S_N2 intermediates at the lowest c.m. collision energies 0.05−0.5 eV. At collision energies above 1 eV, the proton-transfer reaction proceeds through an alternative mechanism via the hydrogen-bonded intermediate. Halophilic attack of the chloromethane is a front-side attack mechanism and may occur at collision energies above 1.8 ± 0.4 eV. The halophilic reaction initially forms only a small FCl^- reaction cross section. At collision energies above 3.6 eV c.m., a new reaction mechanism is postulated via collisionally activated dissociation of the CH_3−Cl bond, resulting in a further increase in the FCl^- cross section. At collision energies >6 eV, the FCl^- reaction cross section starts to decrease with a subsequent increase in the Cl^- reaction cross section, which may be explained by the FCl^- ion dissociating into $F + Cl^-$. An alternative nucleophilic displacement mechanism via front-side attack without inversion of the methyl group is also a possible source of Cl^- at higher energies, but there is no experimental evidence to confirm such a mechanism.

Acknowledgment. We gratefully acknowledge the donors of the Petroleum Research Fund, administered by the American Chemical Society, for partial support of this research. This work is also supported in part by the U.S. Department of Energy, Office of Science, Office of Basic Energy Sciences, Chemical Sciences, Geosciences and Biosciences Division. We thank A. A. Viggiano for supplying numerical values for the VT-SIFDT data in Figure 7.

References and Notes

(1) Chabinyc, M. L.; Craig, S. L.; Regan, C. K.; Brauman, J. I. *Science* **1998**, *279*, 1882.
(2) Hase, W. L. *Science* **1994**, *266*, 998.
(3) Shaik, S. S.; Schlegel, H. B.; Wolfe, S. *Theoretical Aspects of Physical Organic Chemistry: The S_N2 Mechanism*; John Wiley and Sons: New York, 1992.
(4) Olmstead, W. N.; Brauman, J. I. *J. Am. Chem. Soc.* **1977**, *99*, 4219.
(5) Dodd, J. A.; Brauman, J. I. *J. Phys. Chem.* **1986**, *90*, 3559.
(6) Brauman, J. I. *J. Mass Spectrom.* **1995**, *30*, 1649.
(7) Su, T.; Morris, R. A.; Viggiano, A. A.; Paulson, J. F. *J. Phys. Chem.* **1990**, *94*, 8426.
(8) Wang, H.; Hase, W. L. *J. Am. Chem. Soc.* **1997**, *119*, 3093.
(9) Su, T.; Wang, H.; Hase, W. L. *J. Phys. Chem. A* **1998**, *102*, 9819.
(10) DePuy, C. H.; Gronert, S.; Mullin, A.; Bierbaum, V. M. *J. Am. Chem. Soc.* **1990**, *112*, 8650.
(11) O'Hair, R. A.; Davico, G. E.; Hacaloglu, J.; Dang, T. T.; DePuy, C. H.; Bierbaum, V. M. *J. Am. Chem. Soc.* **1994**, *116*, 3609.
(12) Su, T.; Bowers, M. *Int. J. Mass Spectrom. Ion Phys.* **1973**, *12*, 347.
(13) VanOrden, S. L.; Pope, R. M.; Buckner, S. W. *Org. Mass Spectrom.* **1991**, *26*, 1003.
(14) Tachikawa, H.; Igarashi, M. *Chem. Phys. Lett.* **1999**, *303*, 81.
(15) Tachikawa, H. *J. Phys. Chem. A* **2000**, *104*, 497.
(16) Cyr, D. A.; Scarton, M. G.; Wiberg, K. B.; Johnson, M. A.; Nonose, S.; Hirokawa, J.; Tanaka, H.; Kondow, T.; Morris, R. A.; Viggiano, A. A. *J. Am. Chem. Soc.* **1995**, *117*, 1828.
(17) DeTuri, V. F.; Hintz, P. A.; Ervin, K. M. *J. Phys. Chem. A* **1997**, *101*, 5969.
(18) Zellermann, G.; Vietzke, E. *Radiochem. Acta* **1990**, *50*, 107.
(19) Schlegel, H.; Mislow, K.; Bernardi, F.; Bottoni, A. *Theor. Chim. Acta* **1977**, *44*, 245.
(20) Ervin, K. M.; Armentrout, P. B. *J. Chem. Phys.* **1985**, *83*, 166.
(21) Rodgers, M. T.; Ervin, K. M.; Armentrout, P. B. *J. Chem. Phys.* **1997**, *106*, 4499.
(22) Armentrout, P. *Int. J. Mass. Spectrom.* **2000**, *200*, 219.
(23) Herzberg, G. *Molecular Spectra and Molecular Structure II. Infrared and Raman Spectra of Polyatomic Molecules*; Van Nostrand Reinhold: New York, 1945.
(24) Beyer, T. S.; Swinehart, D. F. *Commun. ACM* **1973**, *16*, 379.
(25) Stein, S. E.; Rabinovitch, B. S. *J. Chem. Phys.* **1973**, *58*, 2438.
(26) Stein, S. E.; Rabinovitch, B. S. *Chem. Phys. Lett.* **1977**, *49*, 183.
(27) Chantry, P. J. *J. Chem. Phys.* **1971**, *55*, 2746.
(28) Lifshitz, C.; Wu, R.; Tiernan, T. O.; Terwilleger, D. T. *J. Chem. Phys.* **1978**, *68*, 247.
(29) Armentrout, P. B.; Ervin, K. M. *CRUNCH*; Fortran program.
(30) Taylor, B. N.; Kuyatt, C. *Guidelines for Evaluating and Expressing the Uncertainty of NIST Measurement Results*; NIST Technical Note 1297; National Institute of Standards and Technology: Washington, DC, 1994.
(31) Frisch, M. J.; Trucks, G. W.; Schlegel, H. B.; Scuseria, G. E.; Robb, M. A.; Cheeseman, J. R.; Zakrzewski, V. G.; Montgomery, J. A., Jr.; Stratmann, R. E.; Burant, J. C.; Dapprich, S.; Millam, J. M.; Daniels, A. D.; Kudin, K. N.; Strain, M. C.; Farkas, O.; Tomasi, J.; Barone, V.; Cossi, M.; Cammi, R.; Mennucci, B.; Pomelli, C.; Adamo, C.; Clifford, S.; Ochterski, J.; Petersson, G. A.; Ayala, P. Y.; Cui, Q.; Morokuma, K.; Malick, D. K.; Rabuck, A. D.; Raghavachari, K.; Foresman, J. B.; Cioslowski, J.; Ortiz, J. V.; Stefanov, B. B.; Liu, G.; Liashenko, A.; Piskorz, P.; Komaromi, I.; Gomperts, R.; Martin, R. L.; Fox, D. J.; Keith, T.; Al-Laham, M. A.; Peng, C. Y.; Nanayakkara, A.; Gonzalez, C.; Challacombe, M.; Gill, P. M. W.; Johnson, B.; Chen, W.; Wong, M. W.; Andres, J. L.; Gonzalez, C.; Head-Gordon, M.; Replogle, E. S.; Pople, J. A. *Gaussian98*, Revision A.6; Gaussian, Inc.: Pittsburgh, PA, 1998.
(32) Glukhovtsev, M.; Bach, R.; Pross, A.; Radom, L. *Chem. Phys. Lett.* **1996**, *260*, 558.
(33) Gritsenko, O.; Ensing, B.; Schipper, P.; Baerends, E. *J. Phys. Chem. A* **2000**, *104*, 8558.
(34) Wolfe, S. *Can. J. Chem.* **1984**, *62*, 1465.
(35) Shi, Z.; Boyd, R. J. *J. Am. Chem. Soc.* **1990**, *112*, 6789.
(36) Glukhovtsev, M. N.; Pross, A.; Radom, L. *J. Am. Chem. Soc.* **1996**, *118*, 6273.
(37) Botschwina, P.; Horn, M.; Seeger, S.; Oswald, R. *Ber. Bunsen-Ges. Phys. Chem.* **1997**, *101*, 387.
(38) Su, T. *J. Chem. Phys.* **1994**, *100*, 4703.
(39) Gronert, S. *J. Am. Chem. Soc.* **1991**, *113*, 6041.
(40) Bartmess, J. E. In *NIST Chemistry WebBook, NIST Standard Reference Database Number 69*; Mallard, W. G., Linstrom, P. J., Eds.; National Institute of Standards and Technology: Gaithersburg, MD, Jan 2000 (http://webbook.nist.gov).
(41) Ingemann, S.; Nibbering N. M. M. *J. Chem. Soc., Perkin Trans. 2* **1985**, *837*, 837.
(42) DeTuri, V. F.; Su, M. A.; Ervin, K. M. *J. Phys. Chem. A* **1999**, *103*, 1468.
(43) DeTuri, V.; Ervin, K. To be submitted.
(44) Yencha, A.; Lopes, M.; King, G.; Hochlaf, M.; Song, Y.; Ng, C.-Y. *Faraday Discuss.* **2000**, *115*, 355.
(45) Martin, J.; Hepburn, J. *Faraday Discuss.* **2000**, *115*, 416.
(46) Henchman, M.; Hierl, P. M.; Paulson, J. F. *J. Am. Chem. Soc.* **1985**, *107*, 2812.
(47) Gurvich, L. V.; Veyts, I. V.; Alcock, C. B. *Thermodynamic Properties of Individual Substances*, 4th ed.; Hemisphere Publishing Corp.: New York, 1991.

(48) Barlow, S. E.; Van Doren, J. M.; Bierbaum, V. M. *J. Am. Chem. Soc.* **1988**, *110*, 7240.
(49) Glukhovtsev, M. N.; Pross, A.; Schlegel, H. B.; Bach, R. D.; Radom, L. *J. Am. Chem. Soc.* **1996**, *118*, 11258.
(50) Deng, L.; Branchadell, V.; Ziegler, T. *J. Am. Chem. Soc.* **1994**, *116*, 6, 10645.
(51) *NIST Chemistry WebBook*; NIST Standard Reference Database Number 69; Mallard, W. G., Linstrom, P. J., Eds.; National Institute of Standards and Technology: Gaithersburg, MD, Jan 2000 (http://webbook.nist.gov).
(52) Dispert, H.; Lacmann, K. *Int. J. Mass Spectrom. Ion Phys.* **1978**, *28*, 49.
(53) Harland, P.; Thynne, J. C. J. *J. Phys. Chem.* **1969**, *73*, 4031.
(54) Dudin, A. V.; Gorokhov, L. N.; Baluev, A. V. *Izv. Akad. Nauk SSR Ser. Khim.* **1979**, 2408.
(55) Dispert, H.; Lacmann, K. *Chem. Phys. Lett.* **1977**, *47*, 533.
(56) Rosenstock, H. M. *Int. J. Mass Spectrom. Ion Phys.* **1976**, *20*, 139.
(57) Murray, K. K.; Leopold, D. G.; Miller, T. M.; Lineberger, W. C. *J. Chem. Phys.* **1988**, *89*, 5442.
(58) Nguyen, M. T.; Ha, T.-K. *Chem. Phys. Lett.* **1987**, *136*, 413.
(59) Van Huis, T. J.; Galbraith, J. M.; Schaefer H. F. *Mol. Phys.* **1996**, *89*, 607.
(60) Curtiss, L. A.; Raghavachari, K.; Redfern, P. C.; Rassolov, V.; Pople, J. A. *J. Chem. Phys.* **1998**, *109*, 7764. Supplementary material at http://chemistry.anl.gov/compmat/g3theory.html.
(61) Kolesov, V. *Russ. Chem. Rev.* **1978**, *47*, 1145.
(62) Berry, R.; Burgess, D.; Nyden, M.; Zachariah, M.; Schwartz, M. *J. Phys. Chem.* **1995**, *99*, 17145.
(63) Graul, S. T.; Squires, R. R. *J. Am. Chem. Soc.* **1990**, *112*, 2517.
(64) Gilles, M.; Ervin, K.; Ho, J.; Lineberger, W. *J. Phys. Chem.* **1992**, *96*, 1130.